PCCP

ROYAL SOCIETY OF CHEMISTRY

PAPER

View Article Online
View Journal

Cite this: DOI: 10.1039/d6cp00626d

Scanning tunneling microscopy of ferrocenecarboxylic acid assemblies on Ag(111): a comparison to Au(111)

Benjamin R. Heiner,[a] Kaitlyn M. Handy,[b] Alex L. Walter,[b] Jacob P. Petersen[c] and S. Alex Kandel *[b]

Received 20th February 2026,
Accepted 9th June 2026

DOI: 10.1039/d6cp00626d

rsc.li/pccp

Scanning tunneling microscopy was used to investigate the arrangement of ferrocenecarboxylic acid (FcCOOH) monolayers on the Ag(111) surface. Four distinct structures were observed, none of which had previously been observed on other surfaces. Structural analysis indicates that these assemblies are primarily composed of dimers. VASP calculations support the molecular assignments of the monolayer structures, while ESI-MS experiments confirm that dimers are the predominant species in solution. Of particular note, the cyclic pentamers and aperiodic packing observed for FcCOOH on Au(111) were not observed, despite (1) the similarity of the Ag(111) and Au(111) surfaces in reactivity, flatness, and lattice constant, and (2) prior explanation of the Au(111) monolayer in terms of molecule–molecule interactions alone. It is clear that while the surface does not have a template structure, it has a significant influence on which structures are formed.

1 Introduction

Ferrocenecarboxylic acid (FcCOOH, Fig. 1) deposited on the surface of Au(111) formed the first observed self-assembled molecular quasicrystal, filling the two-dimensional space with local five-fold symmetry.[1] The monolayer, observed by scanning tunneling microscopy (STM), was built using FcCOOH pentamers, which in turn were stabilized by an unusual bonding motif, in the form of cyclic catameric hydrogen bonds.[1–5] These pentamers were intermixed with hydrogen-bonded dimers to create the extended structure. Surface self-assembly is generally described as an interplay between molecule–molecule and molecule–surface interactions, but in the case of FcCOOH on Au(111), the overall features of the monolayer seemed to be well explained only by intermolecular interactions.[1] This was attributed to the relative inertness and smoothness of the Au(111) surface, which was then explained as relatively unimportant given the strength of the hydrogen bonds between molecules. In support of this hypothesis, isolated pentamers were observed to be randomly oriented relative to the surface, indicating a low corrugation of the cluster–surface interaction potential.

We decided to probe whether surface–molecule interactions could in fact be neglected when modeling the quasicrystal structure by comparing assembly on Ag(111), which is also a relatively inert and smooth surface. Ag(111) has a nearly identical lattice constant to Au(111), though the gold surface reconstructs to modify the atomic arrangement slightly.[6] Performing the same

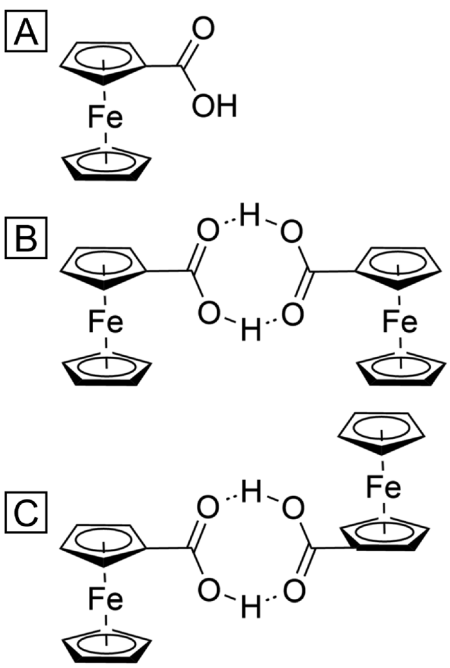

Fig. 1 (A) The molecular structure of ferrocenecarboxylic acid. (B) Two molecules hydrogen-bonded together to form a *cis*-dimer. (C) Two molecules hydrogen-bonded together to form a *trans*-dimer.

Los Alamos National Laboratory, P.O. Box 1663, Los Alamos, NM, 87545, USA
[b] *Department of Chemistry and Biochemistry, University of Notre Dame, Notre Dame, IN, 46556, USA. E-mail: skandel@nd.edu*
[c] *Evident Scientific, Webster, TX, 77598, USA*

experiment as done in ref. 1 but on the Ag(111) surface instead of Au(111), we expected to see the same aperiodic assembly. We did not, and we instead characterized multiple structures distinct from any of those that formed on gold.

Comparison of multiple structures on two different surfaces will also provide insights into complex systems arising from two-dimensional self-assembly and the effect of molecular structure on crystal structure formation.[7–14] We also believe that studying systems where 2-D self-assembly results in multiple complex (metastable) structures will give valuable insights into synergistic interactions between molecular functional groups, and this will have broad impact upon the larger and important problem of crystal structure prediction, specifically the understanding of crystal polymorphism.[15–17]

2 Methods

An Ag(111) single crystal was cleaned in a high vacuum with three cycles of Ar^+ sputtering (0.55 kV for 15 minutes) and subsequently annealed at approximately 390 °C, which was found to yield flat, clean surfaces of Ag(111). Cleaned samples were allowed to cool before being transferred to a load-lock chamber for preparation of the monolayer. FcCOOH was purchased from Sigma Aldrich and used without further purification. Solutions with a concentration of 10 mM were prepared in either benzene or toluene (noted in figures). The FcCOOH solution was deposited *via* a pulsed-solenoid valve (Parker Instruments, Series 9, Iota One Driver, 0.5 mm diameter nozzle) onto the cleaned Ag(111) substrate. The substrate was at room temperature at the time of deposition. Before the deposition, the load-lock chamber was at a pressure of $<5 \times 10^{-6}$ Torr. The pressure rose significantly, by about an order of magnitude, then returned to the baseline pressure within a minute. The sample was then transferred to an Omicron LT-STM, kept at a base pressure of 5×10^{-10} Torr, and was cooled to 77 K using liquid nitrogen. All images were acquired with a Pt/Ir tip in constant current mode with a tunneling current of 10 pA and a tip–sample bias of +1.0 V unless otherwise noted.

The STM was regularly calibrated throughout the study using images of the Au(111) herringbone reconstruction. Measurement and unit cell analysis were performed using the WSxM software package.[18]

Molecular models were built by geometrically optimizing monomers and dimers of FcCOOH using density functional theory (DFT). Optimization studies were performed in the Gaussian 16 software package at the B3LYP/6-31g(d) level of theory.[19] Optimization began with a bias toward either the *cis* or *trans* orientation, allowing for the more energetic *cis* and less energetic *trans* orientation to be optimized to local energy minima. Optimized measurements were visualized using the IQMol software package and used as the monomer and dimer models in the study.[20] Models were placed on the calibrated STM images at size with zero degrees of freedom; the models had no adjustable parameters or flexibility in size, orientation, or conformation.

The predicted STM images were simulated utilizing VASP.[21–24] A slab of Ag(111) was constructed with the dimensions of $7 \times 7 \times 4$ silver atoms with 10 Å of vacuum above and below the slab. No atoms were frozen during relaxation of the slab. The lattice constant was found to be 4.2 Å. All single-point calculations for the silver slab were conducted with an energy cutoff (encut) of 550 eV. All other calculations were conducted with a PBE functional with an encut of 500 eV. The k points used were [7, 7, 1] with an energy difference of 1×10^{-5} eV. A van der Waals correction IVDW = 11 was added.[25,26] Bader charge analysis (see the SI) was performed according to ref. 27–29.

All ESI-MS experiments were performed on a Waters ACQUITY tandem triple quadrupole mass spectrometer (MS). The MS is equipped with a ZSpray electrospray ionization source. 1.7 mM FcCOOH/methanol solutions were directly infused into the instrument at a rate of 10 μL min^{-1} through a syringe pump. Spectra were collected in both positive and negative mode and are labeled with their respective polarity. Operating conditions follow ref. 2 capillary voltage was set to 3.6 kV, cone voltage to 25 V, source and desolvation temperatures to 50 °C, and desolvation gas flow to 300 L h^{-1}. All spectra were acquired over 10 minutes, at a scan rate of 3 s per scan, totaling about 200 scans, and are additive. Daughter scans were acquired under the same conditions.

Spectra were normalized to their tallest peaks (the –/+ H monomer peaks).[30] All peaks were isotopically identified. The limit of detection was determined by 3.3 times the root mean square of a blank methanol measurement under the same mass spectrometer conditions.

3 Results and discussion

Pulse deposition onto Ag(111) resulted in four monolayer structures not found during any Au(111) study. The most stable, or the most common, configuration of FcCOOH on Ag(111) is the honeycomb-like surface in Fig. 2. This configuration has a number of interesting features, most notably a ''dimple'' of electron density at molecule sites and a dim feature packed inside of the honeycomb. The dimple feature is qualitatively different from other configurations of FcCOOH on Ag(111), mainly the molecular area of electron density is smaller and the dimple feature at the center of the molecule appears at lower contrast than in other configurations. A similar feature was seen while studying iron-containing organic metallic frameworks and diferrocenylacetylene.[5,31] Predicted diferrocenylacetylene STM images revealed that when the cyclopentadiene (Cp) rings of the ferrocenes were imaged at increasing angles, the dimpling in the STM images would get smaller, with the dip of electron density becoming less pronounced. Using this information, we conclude that the Cp rings of the FcCOOH in Fig. 2 are likely at an angle to the surface of Ag(111). This conclusion is in agreement with XRD measurements of FcCOOH, which reveal that the structure of the bulk crystal is an assembly of dimers in the *trans* configuration.[32] *trans* dimers of FcCOOH on a flat surface, oriented to maximize Cp interaction with the surface of the substrate, would result in the Cp rings being imaged at a slight angle as both Cp rings in a *trans* dimer cannot be both parallel and close to the surface.

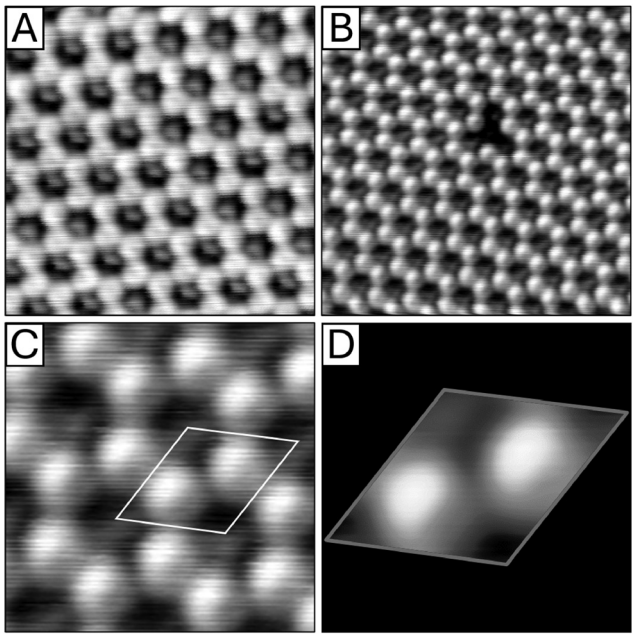

Fig. 2 (A) STM image (87.5 × 87.5 Å) of FcCOOH pulse deposited in benzene on the Ag(111) surface. (B) STM image (125 × 125 Å) of FcCOOH pulse deposited in benzene on the Ag(111) surface. (C) STM image (30 × 30 Å) of a single grain boundary from (B). (D) Unit cell of the honeycomb assembly created by averaging all the unit cells from a single grain boundary from (B). The unit cell rhombus measures 14 × 14.5 Å and 58.6°. While the benzene is the solvent in these images, this assembly also appears when deposited in toluene (Fig. S1).

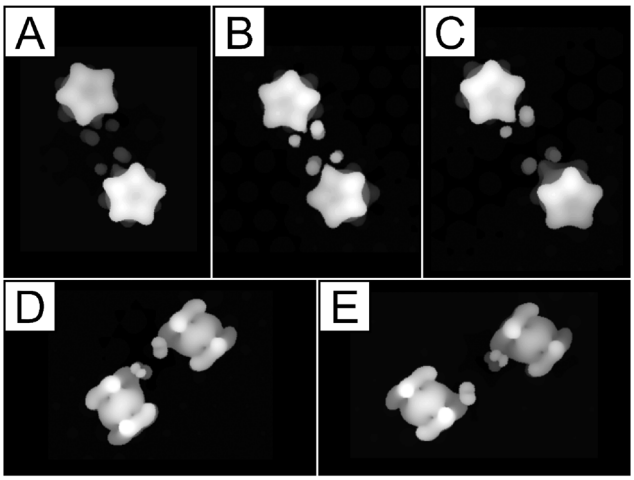

Fig. 3 VASP predicted STM images of (A) *cis* dimer with Cp rings parallel to the surface, COOH group down, (B) *cis* dimer with Cp rings parallel to the surface, COOH group up, (C) *trans* dimer with Cp rings as parallel as possible to the surface, (D) *cis* dimer with Cp rings perpendicular to the surface, and (E) *trans* dimer with Cp rings perpendicular to the surface.

To help differentiate between FcCOOH dimers in different orientations, we predicted *via* simulations, STM images of *cis* dimers with the Cp rings parallel to the surface with the carboxylic acid (COOH) group facing both toward and away from the surface: a *cis* dimer with the Cp rings perpendicular to the surface, and *trans* dimers with the Cp rings both perpendicular and parallel to the surface. The results in Fig. 3 are consistent with the conclusions from the diferrocenylacetylene calculations, that is, that dimples of electron density would be seen while the Cp rings are perpendicular to the scan direction (A–B). Additionally, the dimpling is expected to be smaller when the *trans* dimers are as close to being perpendicular as possible (Fig. 3C). The comparison of these simulated STM images supports our interpretation of the FcCOOH orientation in Fig. 2 as *trans* dimers oriented to maximize Cp interactions with the surface. The calculations of *cis* and *trans* dimers with Cp rings perpendicular to the surface (Fig. 3D and E) are used for orientation and iron–iron distance measurements, which will be used later for other surface assignments.

To better understand which orientation of FcCOOH is most energetically stable, we calculated single point energies of each dimer to compare which distance from the surface is predicted to be most favorable (Fig. 4). Interestingly, both the *cis* and *trans* dimers possessed nearly identical predicted binding energies at iron–surface distances between 5.5 and 6.0 Å. The calculations predict that the orientation of the Cp rings and the COOH group is relatively insignificant and that iron has a far greater influence on binding distance than any other factor in the molecule or the dimer. Based on these calculations, we also conclude that every one of these dimer orientations is energetically competitive on the surface, allowing for many different orientations and interdimer interactions.

The dimple feature in the center of the honeycomb varies in brightness from image to image (Fig. 2A and B). We believe this to be mainly a parameter of the tip condition, as differences in the structure of the STM images from one experiment to the next are well known to cause variation in image contrast. Previous studies concerning ferrocenes have revealed that ferrocenes on the surface of gold appear less bright when oriented with Cp rings perpendicular to the surface, so we conclude that those features are the same.[1–5] We also observe that the FcCOOH molecule packing on the inside of the honeycomb structure has two orientations, up and down, as seen in Fig. 2A. As the monomer has an non-hydrogen-bonded COOH group, chemical reasoning suggests that it would be interacting with the π structures in an adjacent Cp ring.

In order to understand the adsorption geometries responsible for different features in STM images, we used DFT-optimized molecular models placed at size onto calibrated STM images. The *trans* dimer was calculated to have an iron–iron distance of 9.67 Å, which agrees very well with the XRD solution, which shows the iron–iron distance to be 9.600 Å.[32] The XRD measured distance was used to assign molecules as seen in Fig. 5A and B. We interpret the honeycomb as *trans* dimers arranged to leave a cavity between them. Even though the surface seems to have six-fold symmetry, the unit cell for the surface, Fig. 2C and D, only contains the dimer. If the dimers were in the *cis* configuration, we would expect three equivalent positions for the monomer to interact with as all the Cp rings would be equivalently parallel to the surface. This is not the case for the *trans* configuration, where only two equivalent positions would exist for the monomer to interact with. This further supports the conclusion that the dimers are in a *trans* configuration.

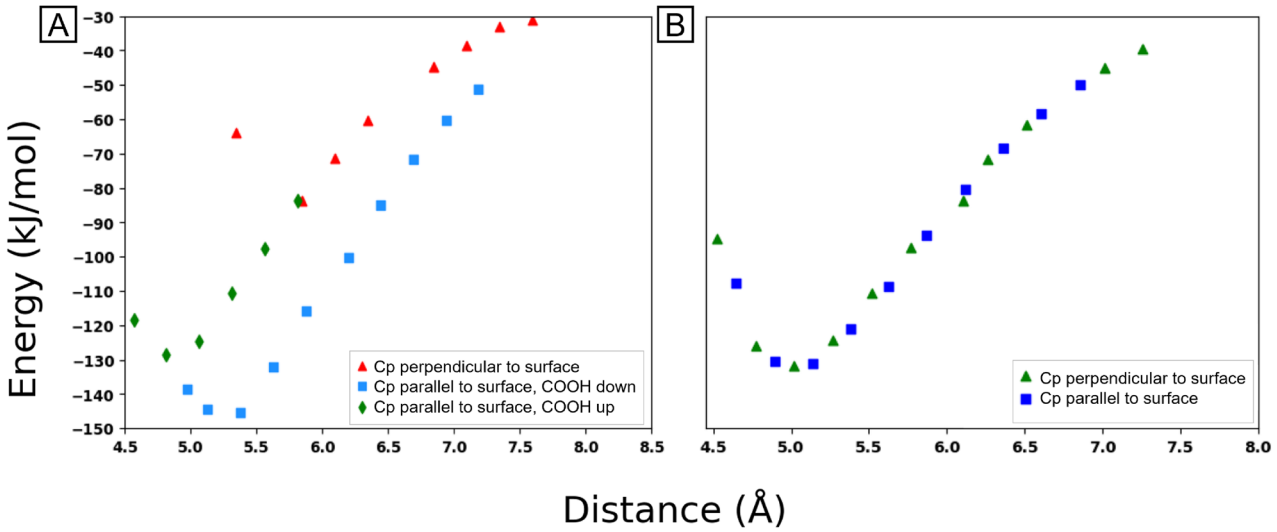

Fig. 4 Calculated adsorption energies for FcCOOH dimers onto the surface of Ag(111) using VASP. Distances are measured from the iron atom to the closest silver atom. (A) *cis* FcCOOH dimers and (B) *trans* FcCOOH dimers.

Many of the images of the honeycomb structure have defects, *i.e.* Fig. 2, Fig. 2B, and especially Fig. 5B. How a model explains the defects and grain boundaries of an assembly can test the validity of the model. This can be seen in Fig. 5B, where there are a large number of defects, which are caused by different orientations of dimers in close proximity to each other. The smaller defects, such as those in Fig. 5A, are more subtle. It is difficult to elucidate the exact orientations of the dimers in these situations, but the small defect indicates that the orientations of the dimers shift by 120. The model that we built using the previously mentioned assumptions describes the surface of this honeycomb-shaped dimer packing very well.

When we measure the angle between the honeycomb lattice and step edges in the Ag(111) surface, the angle is consistently 60. This is evidence that the FcCOOH lattice and the Ag(111) surface lattice are commensurate and suggests that surface–molecule interactions affect FcCOOH self-assembly, which was not the case for the quasicrystalline structure on Au(111).

The second assembly seems to be a combination of arrangements of ferrocenecarboxylic acid dimers (Fig. 6). The molecules that appear round have the familiar dimple feature, but they are different from those seen in Fig. 2. These are larger and have a darker center, which is seen in the unit cell (Fig. 6). We therefore interpret these features as Cp rings parallel to the surface of the silver. These contrast changes were also seen in simulated STM images of diferrocenylacetylene, which predicted that perpendicular imaging of a Cp ring would result in a distinct, bright ring of electron density with a dim feature in the middle.[5] Again, our calculations (Fig. 3A and B) are in agreement. The round features are interpreted as ferrocenecarboxylic acid molecules hydrogen bonded in the *cis* formation with the Cp rings parallel to the surface. In between these rows of *cis* dimers are smaller, dimmer features. The shape and

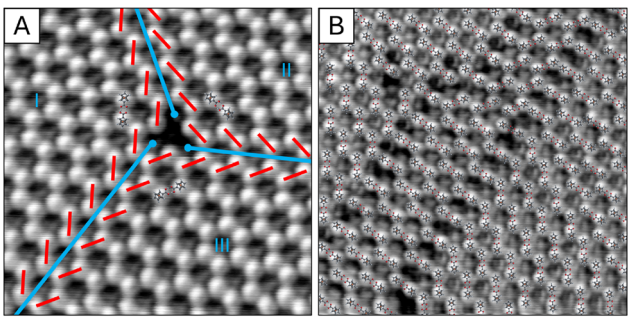

Fig. 5 (A) Assignment of the molecules on the image from Fig. 2 based on our interpretations and observations of the honeycomb assembly. The grain boundaries marked by the molecular vacancy are shown in blue. Representative molecular models of the *trans* dimer are shown in each region in the correct orientation with the red lines indicating dimerized molecules along the grain boundary. (B) Our model holds as we extend it to images of larger fields with more defects (150 × 150 Å). In fact, more defects in the image clarifies molecular orientation.

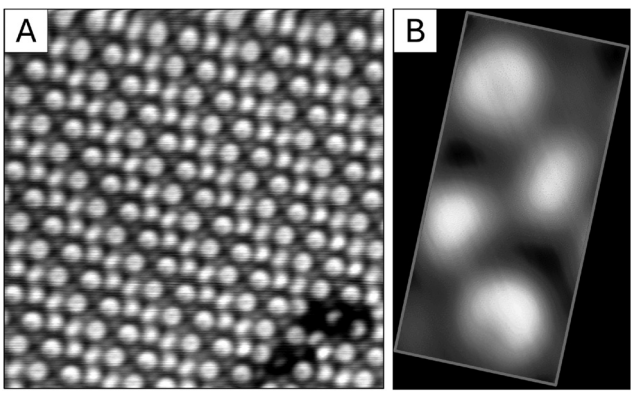

Fig. 6 (A) STM image (150 × 150 Å) of FcCOOH pulse deposited in toluene on Ag(111). (B) Unit cell (12 × 28 Å and 91.3°) of the stripe packing created by averaging all the unit cells from (A). The unit cell contains four molecules, two oriented with the Cp rings parallel to the surface, and two perpendicular.

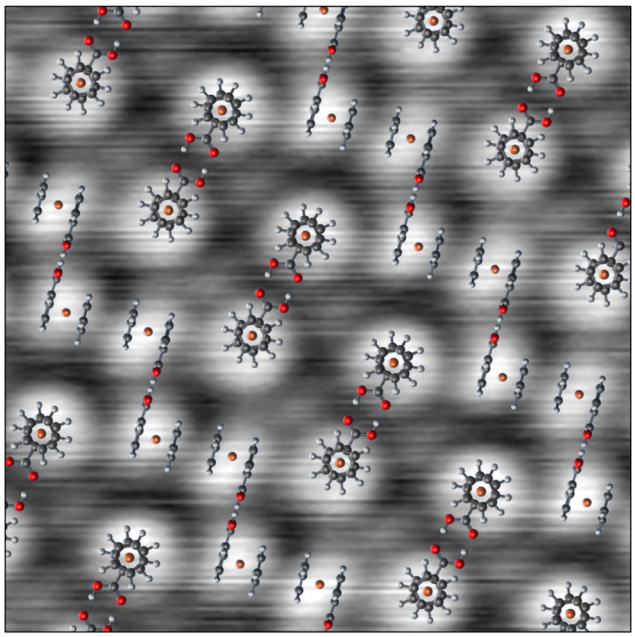

Fig. 7 A magnified (60 × 60 Å) image from Fig. 6a with molecular assignment for the stripes assembly placed on the image.

orientation of these features match well with our VASP simulated images of a *trans* dimer with Cp rings perpendicular to the surface (Fig. 3C).

cis dimers do not appear in XRD measurements, so we rely on the DFT calculated Fe–Fe distance, 9.07 Å, to make molecular assignments to this surface. Fig. 7 shows how the *cis* dimers and the perpendicular *trans* dimers arrange to form the assembly image in Fig. 6.

The third assembly, Fig. 8 is similar to the previous one, but the unit cell is distinctly different. In the creation of the unit cell, we found that the two rows highlighted in Fig. 8A in blue and red are not equivalent. This makes the unit cell long and narrow, Fig. 8B. Molecular features in this configuration appear at distances that are not consistent with FcCOOH dimers, and we are not able to suggest a chemically plausible structure that would produce this experimental image.

The final assembly does not appear to be formed from dimers (Fig. 9). The images show round molecules with dimple features, but each molecule has a tail of electron density. The dimple is very similar to that seen in Fig. 6, so we interpret the FcCOOH molecules as being oriented with the Cp rings parallel to the surface. The image shows that this assembly is formed from molecules tightly packed into rows with tails of electron density maintaining directionality through the row. The tail switches direction consistently in every row and appears in every image of this assembly, so we can conclude that it is a real feature, making the unit cell contain two differently oriented molecules (Fig. 9B). We interpret the tail as the carboxylic acid of the FcCOOH oriented to interact with the π system of adjacent molecules, shown in the molecular assignment in Fig. 10.

None of the four discussed assemblies of FcCOOH on Ag(111) form when experiments are performed on Au(111).

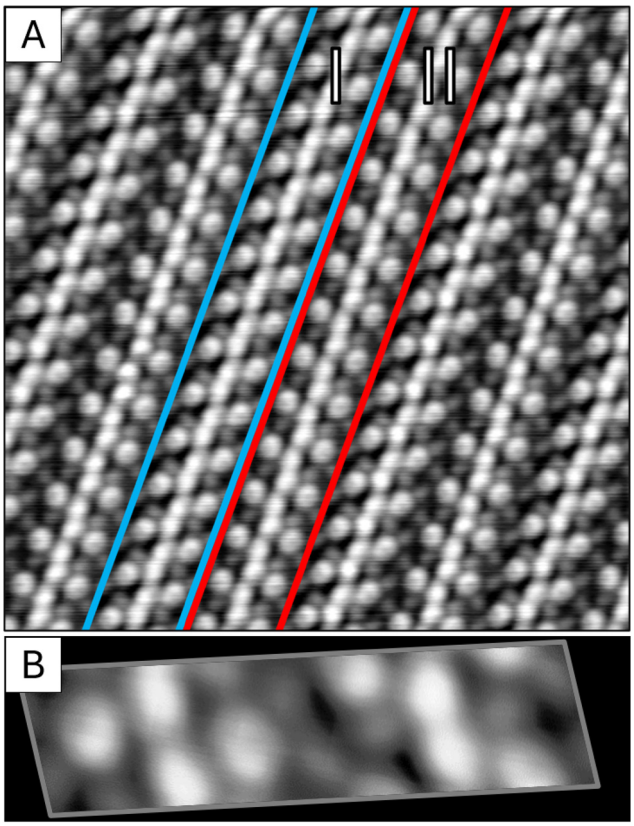

Fig. 8 (A) STM image (212.5 × 212.5 Å) of FcCOOH pulse deposited in toluene on Ag(111). The rows of molecules marked in blue and those in red are not in the same orientation as the blue and red areas do not share equivalent molecules. (B) Unit cell (16.9 × 61.9 Å and 80.5°) of the assembly created by averaging all the unit cells from (A).

Additionally, none of the assemblies previously observed, including the quasicrystalline surface, were observed on using Ag(111) as a substrate. A full model of these systems is still not understood as discussions and assignments are centered primarily on molecule–molecule interactions, without taking into

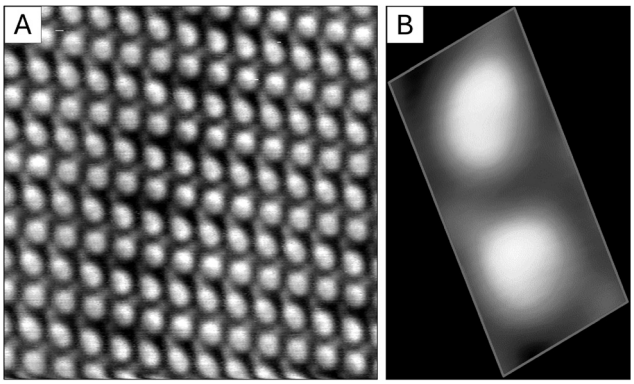

Fig. 9 (A) STM image (125 × 125 Å) of FcCOOH pulse deposited in benzene on Ag(111). (B) Unit cell (10 × 22 Å and 80.4°) of the teardrop assembly. There is a tail of electron density that appears to be interacting with neighboring molecules, which is interpreted as the carboxylic acid interacting with the Cp rings of the neighboring molecule.

consideration molecule–surface interactions. We cannot conclude that the identity of the surface is important in all cases, but for FcCOOH, at least one or both the Au(111) and Ag(111) surfaces clearly affect the outcome of the experiment. One of the surfaces may not influence the self-assembly of FcCOOH, but it is not possible that both do not. Based on the commensurate nature of the FcCOOH surface in Fig. 2, we conclude the surface interactions for Ag(111) to be more significant than those in Au(111).

Previous work from our research group has demonstrated that the preparation of monolayers using pulse deposition often results in a combination of multiple cluster geometries and monolayer structures that are not observed after vapor deposition of the same molecule.[15] This has led us to hypothesize that molecules can pre-associate in solution and deposit onto a surface as clusters. We have employed ESI-MS to test this model, and have found in several cases that "magic number" clusters formed preferentially during the electrospray process corresponding to cluster sizes observed in STM images of the surface.[2,33–35] Fig. 12A shows clustering of FcCOOH using ESI-MS in the negative mode. The spectrum shows the dimer being nearly as abundant as the monomer. The positive mode spectrum (Fig. 12b) also shows clustering of the dimer, trimer, and tetramer, with the tetramer showing the most abundance of those clusters. In addition, cluster with Na or NH_4 adducts (which come from impurities in the methanol mobile phase) become more common than simply protonated clusters. The change in the adduct is due to the FcCOOH being a partially deprotonated weak acid in methanol, which becomes undetectable using MS with the addition of a proton.

The dimers and tetramers indicate a polarity dependence because samples were made in acetonitrile, yet the tetramer still clusters strongly in the positive mode (SI1). Interestingly, the protonated clusters show the expected exponential decay as cluster size increases,[34–39] while sodiated clusters remain prevalent through trimers and tetramers (Fig. 12c). Daughter scans of the sodiated tetramer (Fig. 12d) show a high abundance of dimers, with some monomers, trimers, and tetramers. We interpret the high abundance of dimers as the tetramers forming from dimeric subunits clustering together to distribute the positive charge.

Notably, no pentamers are observed in either polarity. Previous studies hypothesized that FcCOOH pentamers formed in solution and that dimers nucleated on the Au(111) surface.[4] However, ESI-MS results indicate that only dimers form in solution, suggesting that the pentamers previously observed arise from surface-driven assembly rather than pre-existing solution-phase clusters. Additional support for this conclusion comes from experiments on the Ag(111) surface, where no pentamers are found, and unit cells instead consist of dimers in various conformations (Fig. 11. This implies that surface interactions play a crucial role in dictating the final assembly, with structural differences between Ag(111) and Au(111) arising from variations in adsorption configurations. A key uncertainty, however, is whether the conditions of electrospray ionization are truly comparable to those of pulse deposition.

Adduct formation plays a key role in cluster stability. Large ions can stabilize clusters that are otherwise less stable,[40–42] leading to the observation of clusters that are energetically less favorable compared to protonated ones. Additionally, intermolecular interactions can be stabilized by charge, as seen with sodium ion stabilization,[40,41] and neutral serine octamers,[43–47] highlighting the influence of charge distribution on clustering behavior. Differences between positive and negative mode clustering are particularly notable. Magic numbers in mass spectra depend more on charge delocalization and the feasibility of adding a charge to a cluster – the easier it is to delocalize the charge, the more likely it is for the cluster to form.[48,49]

Steric effects also contribute to clustering behavior, potentially influencing the observed distributions.[50] Additionally, different models have been proposed to describe cluster size distributions, with some studies supporting exponential decay,[34–39] while others suggest Gaussian distributions.[51,52]

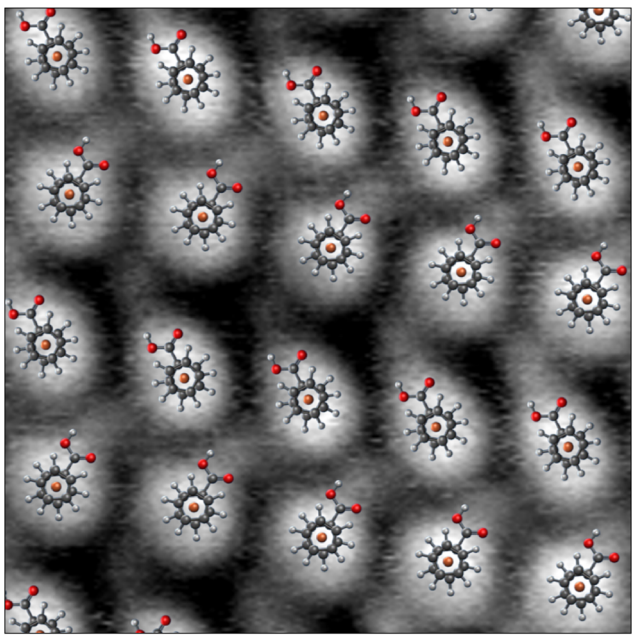

Fig. 10 A magnified (45 × 45 Å) image from Fig. 9a with molecular assignment for the teardrop assembly placed on the image.

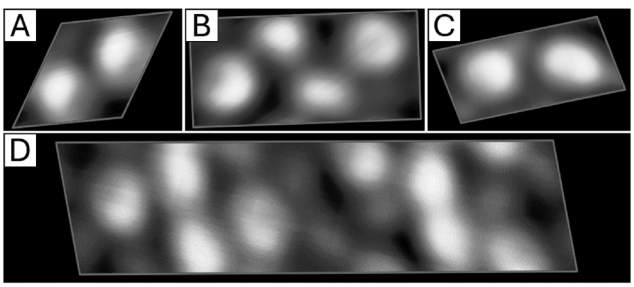

Fig. 11 Unit cells from each of the four assemblies ((A) honeycomb (Fig. 2), (B) stripes (Fig. 6), (C) teardrop (Fig. 9), and (D) the V formation (Fig. 8)) of FcCOOH on Ag(111) calibrated to each other in length.

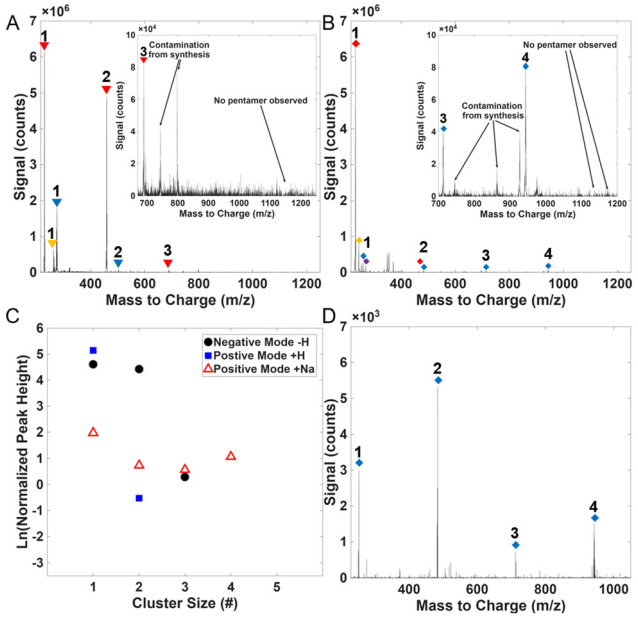

Fig. 12 Mass spectra of FcCOOH. Insets are the regions from 700 to 1250 *m/z*. (A) Negative mode mass spectrum with peaks labeled by number. The color of the triangles dictates the different adducts: red is the loss of a proton, yellow is the addition of a chloride ion, and blue is the addition of a formic acid ion and the loss of two protons. (B) Positive mode spectrum with peaks labeled by number. The color of the diamonds dictates the different adducts: red is the addition of a proton, yellow is the addition of an ammonium ion, blue is the addition of a sodium ion, and purple is the addition of a potassium ion. (C) Natural logarithm of the normalized peak height vs the cluster sizes in spectra (A) and (B). (D) Daughter scan of the FcCOOH sodiated tetramer seen in (B). The dimer is the most prominent peak, indicating that the tetramer is made up of dimeric subunits.

Ferrocene (Fc), under the same experimental ESI conditions, does not exhibit the same clustering behavior as FcCOOH (see the SI, Fig. S2a). The monomer is the dominant peak, and the dimer is only observed as a non-protonated ammonium adduct, indicating that the carboxylic acid facilitates the hydrogen bonding of the dimers both in solution and on surfaces. Fc ionizes very poorly in the negative mode, as there is no readily apparent site for a proton to be removed or for a negatively charged adduct to be stably attached, so only positive mode scans were performed. When graphing the natural log of the peak heights (SI2b), there was no protonated dimer to compare to, so the dimer with the ammonium adduct was used. The lack of protonated dimer and tetramer in the spectrum shows that the carboxylic acid drives dimerization, almost certainly through hydrogen bonding.

4 Conclusions

In this study, we have characterized a new FcCOOH self-assembled system and observed significant polymorphism, highlighting the complexity of FcCOOH assemblies. By comparing FcCOOH behavior on Au(111) and Ag(111), we demonstrate that surface interactions play a role in the final monolayer structure for at least one of the two surfaces. We conclude that based on the commensurate nature of the periodic systems to the Ag(111) *versus* the aperiodic assembly on Au(111), molecule–surface interactions are stronger and play a more significant role for Ag(111). Due to the lack of pentamers in the ESI-MS measurements, Au(111) surface interactions are either meaningful and drive pentamer formation, or the energetics of forming cyclical catamers far outweigh those of the surface interactions.

While our molecular models successfully describe the observed assemblies based on molecule–molecule interactions, our results suggest that this approach alone provides an incomplete picture. The differences in assemblies formed on Au(111) and Ag(111) indicate that molecule–surface interactions contribute meaningfully to the self-assembly process, challenging the assumption that they can be ignored when strong intermolecular forces are present. Further investigation into how subtle variations in surface properties influence molecular self-assembly could provide more insight into the role of surface effects in molecular self-assembly, including those on other faces of gold and silver, HOPG, and especially on Cu(111). We anticipate that further characterization studies may yield yet unseen FcCOOH polymorphs but will likely share similar geometries to those characterized here as those are driven by the strong carboxylic acid hydrogen bond interactions that would be present in every system.

Conflicts of interest

There are no conflicts to declare.

Data availability

Data for this article, including the scanning tunneling microscopy images, are available on the Kandel Group website at https://graphite.chemistry.nd.edu/. Theoretical result data for this article are available at https://doi.org/10.7910/dvn/xqycpl.

Supplementary information (SI) is available. See DOI: https://doi.org/10.1039/d6cp00626d.

Acknowledgements

At Notre Dame, support for this work was from the National Science Foundation (NSF Grants No. CHE-1807313 and CHE-2108186). At LANL, this work was supported by the U.S. Department of Energy, Office of Science, Office of Basic Energy Sciences, Heavy Element Chemistry Program under Early Career FWP No. EC2021LANL05 (LA-UR-26-20801).

References

1 N. A. Wasio, R. C. Quardokus, R. P. Forrest, C. S. Lent, S. A. Corcelli, J. A. Christie, K. W. Henderson and S. A. Kandel, *Nature*, 2014, **507**, 86–89.
2 R. D. Brown, J. M. Coman, J. A. Christie, R. P. Forrest, C. S. Lent, S. A. Corcelli, K. W. Henderson and S. A. Kandel, *J. Phys. Chem. C*, 2017, **121**, 6191–6198.

3 R. C. Quardokus, N. A. Wasio, R. D. Brown, J. A. Christie, K. W. Henderson, R. P. Forrest, C. S. Lent, S. A. Corcelli and S. Alex Kandel, *J. Chem. Phys.*, 2015, **142**, 101927.
4 R. C. Quardokus, N. A. Wasio, J. A. Christie, K. W. Henderson, R. P. Forrest, C. S. Lent, S. A. Corcelli and S. Alex Kandel, *Chem. Commun.*, 2014, **50**, 10229–10232.
5 R. C. Quardokus, N. A. Wasio, R. P. Forrest, C. S. Lent, S. A. Corcelli, J. A. Christie, K. W. Henderson and S. Alex Kandel, *Phys. Chem. Chem. Phys.*, 2013, **15**, 6973–6981.
6 P. Li and F. Ding, *Sci. Adv.*, 2022, **8**, eabq2900.
7 L. Dong, Z. Gao and N. Lin, *Prog. Surf. Sci.*, 2016, **91**, 101–135.
8 G. R. Desiraju, *J. Am. Chem. Soc.*, 2013, **135**, 9952–9967.
9 S. De Feyter and F. C. De Schryver, *Chem. Soc. Rev.*, 2003, **32**, 139–150.
10 R. Xie, Y. Hu and S.-L. Lee, *Small*, 2023, **19**, 2300413.
11 T. Kudernac, S. Lei, J. A. A. W. Elemans and S. De Feyter, *Chem. Soc. Rev.*, 2009, **38**, 402–421.
12 R. Otero, J. M. Gallego, A. L. V. de Parga, N. Martín and R. Miranda, *Adv. Mater.*, 2011, **23**, 5148–5176.
13 C. G. Ayani, M. Pisarra, J. I. Urgel, J. J. Navarro, C. Díaz, H. Hayashi, H. Yamada, F. Calleja, R. Miranda, R. Fasel, F. Martín and A. L. Vázquez de Parga, *Nanoscale Horiz.*, 2021, **6**, 744–750.
14 S. Hennessey, R. González-Gómez, N. Arisnabarreta, A. Ciotti, J. Hou, N. V. Tarakina, A. Bezrukov, K. S. Mali, M. Zaworotko, S. De Feyter, M. García-Melchor and P. Farràs, *Adv. Mater.*, 2025, **37**, 2502155.
15 B. R. Heiner, A. M. Pittsford and S. A. Kandel, *Chem. Commun.*, 2023, **59**, 170–178.
16 B. R. Heiner, K. M. Handy, A. M. Devlin, J. L. Soucek, A. M. Pittsford, D. A. Turner, J. P. Petersen, A. G. Oliver, S. A. Corcelli and S. A. Kandel, *Phys. Chem. Chem. Phys.*, 2024, **26**, 25430–25438.
17 Y. Hu, S.-L. Lee, K. Tahara and S. De Feyter, *J. Phys. Chem. C*, 2024, **128**, 11896–11903.
18 I. Horcas, R. Fernández, J. M. Gómez-Rodríguez, J. Colchero, J. Gómez-Herrero and A. M. Baro, *Rev. Sci. Instrum.*, 2007, **78**, 013705.
19 M. J. Frisch, G. W. Trucks, H. B. Schlegel, G. E. Scuseria, M. A. Robb, J. R. Cheeseman, G. Scalmani, V. Barone, G. A. Petersson, H. Nakatsuji, X. Li, M. Caricato, A. V. Marenich, J. Bloino, B. G. Janesko, R. Gomperts, B. Mennucci, H. P. Hratchian, J. V. Ortiz, A. F. Izmaylov, J. L. Sonnenberg, D. Williams-Young, F. Ding, F. Lipparini, F. Egidi, J. Goings, B. Peng, A. Petrone, T. Henderson, D. Ranasinghe, V. G. Zakrzewski, J. Gao, N. Rega, G. Zheng, W. Liang, M. Hada, M. Ehara, K. Toyota, R. Fukuda, J. Hasegawa, M. Ishida, T. Nakajima, Y. Honda, O. Kitao, H. Nakai, T. Vreven, K. Throssell, J. A. Montgomery Jr, J. E. Peralta, F. Ogliaro, M. J. Bearpark, J. J. Heyd, E. N. Brothers, K. N. Kudin, V. N. Staroverov, T. A. Keith, R. Kobayashi, J. Normand, K. Raghavachari, A. P. Rendell, J. C. Burant, S. S. Iyengar, J. Tomasi, M. Cossi, J. M. Millam, M. Klene, C. Adamo, R. Cammi, J. W. Ochterski, R. L. Martin, K. Morokuma, O. Farkas, J. B. Foresman and D. J. Fox, *Gaussian 16, Revision C.01*, 2016, Gaussian Inc., Wallingford CT.
20 A. Gilbert, *IQmol molecular viewer*, 2012.
21 G. Kresse and J. Hafner, *Phys. Rev. B:Condens. Matter Mater. Phys.*, 1993, **47**, 558–561.
22 G. Kresse and J. Hafner, *Phys. Rev. B:Condens. Matter Mater. Phys.*, 1994, **49**, 14251–14269.
23 G. Kresse and J. Furthmüller, *Comput. Mater. Sci.*, 1996, **6**, 15–50.
24 G. Kresse and J. Furthmüller, *Phys. Rev. B:Condens. Matter Mater. Phys.*, 1996, **54**, 11169–11186.
25 S. Grimme, *J. Comput. Chem.*, 2006, **27**, 1787–1799.
26 S. Grimme, J. Antony, S. Ehrlich and H. Krieg, *J. Chem. Phys.*, 2010, **132**, 154104.
27 W. Tang, E. Sanville and G. Henkelman, *J. Phys.: Condens. Matter*, 2009, **21**, 084204.
28 E. Sanville, S. D. Kenny, R. Smith and G. Henkelman, *J. Comput. Chem.*, 2007, **28**, 899–908.
29 G. Henkelman, A. Arnaldsson and H. Jónsson, *Comput. Mater. Sci.*, 2006, **36**, 354–360.
30 MATLAB, version R2024a, The MathWorks Inc., Natick, Massachusetts, 2024.
31 N. Arisnabarreta, Y. Hao, E. Jin, A. Salamé, K. Muellen, M. Robert, R. Lazzaroni, S. Van Aert, K. S. Mali and S. De Feyter, *Adv. Energy Mater.*, 2024, **14**, 2304371.
32 F. A. Cotton and A. H. Reid, *Acta Crystallogr., Sect. C:Cryst. Struct. Commun.*, 1985, **41**, 686–688.
33 A. M. Silski-Devlin, J. P. Petersen, J. Liu, G. A. Turner, J. C. Poutsma and S. A. Kandel, *J. Phys. Chem. C*, 2020, **124**, 5213–5219.
34 A. M. Silski, R. D. Brown, J. P. Petersen, J. M. Coman, D. A. Turner, Z. M. Smith, S. A. Corcelli, J. C. Poutsma and S. A. Kandel, *J. Phys. Chem. C*, 2017, **121**, 21520–21526.
35 R. D. Brown, S. A. Corcelli and S. A. Kandel, *Acc. Chem. Res.*, 2018, **51**, 465–474.
36 D. Zhang, L. Wu, K. J. Koch and R. G. Cooks, *Eur. Mass Spectrom.*, 1999, **5**, 353–361.
37 A. M. Silski-Devlin, J. P. Petersen, J. Liu, S. A. Corcelli and S. A. Kandel, *J. Phys. Chem. C*, 2020, **124**, 17717–17725.
38 F. C. Gozzo, L. S. Santos, R. Augusti, C. S. Consorti, J. Dupont and M. N. Eberlin, *Chem. – Eur. J.*, 2004, **10**, 6187–6193.
39 S. Wong and F. Röllgen, *Int. J. Mass Spectrom. Ion Processes*, 1986, **70**, 135–144.
40 E.-L. Zins, *J. Mass Spectrom.*, 2013, **48**, 438–447.
41 M. Frańska, *Rapid Commun. Mass Spectrom.*, 2013, **27**, 2823–2827.
42 J. Seo, S. Warnke, K. Pagel, M. T. Bowers and G. von Helden, *Nat. Chem.*, 2017, **9**, 1263–1268.
43 X. F. D. Chillier, A. Monnier, H. Bill, F. O. Gülaçar, A. Buchs, S. A. McLuckey and G. J. Van Berkel, *Rapid Commun. Mass Spectrom.*, 1996, **10**, 299–304.
44 J. S. Jordan and E. R. Williams, *Anal. Chem.*, 2021, **93**, 1725–1731.
45 R. G. Cooks, D. Zhang, K. J. Koch, F. C. Gozzo and M. N. Eberlin, *Anal. Chem.*, 2001, **73**, 3646–3655.
46 A. D. Jacobs, K. V. Jovan Jose, R. Horness, K. Raghavachari, M. C. Thielges and D. E. Clemmer, *J. Am. Soc. Mass Spectrom.*, 2018, **29**, 95–102.

47 R. Chen, Z. Wei and R. G. Cooks, *Anal. Chem.*, 2021, **93**, 1092–1099.
48 P. Liigand, K. Kaupmees, K. Haav, J. Liigand, I. Leito, M. Girod, R. Antoine and A. Kruve, *Anal. Chem.*, 2017, **89**, 5665–5668.
49 P. Liigand, A. Heering (Suu), K. Kaupmees, I. Leito, M. Girod, R. Antoine and A. Kruve, *J. Am. Soc. Mass Spectrom.*, 2017, **28**, 2124–2131.
50 N. Lentz and R. Houk, *J. Am. Soc. Mass Spectrom.*, 2007, **18**, 285–293.
51 S. E. Rodriguez-Cruz, J. S. Klassen and E. R. Williams, *J. Am. Soc. Mass Spectrom.*, 1997, **8**, 565–568.
52 D. Zhang and R. Cooks, *Int. J. Mass Spectrom.*, 2000, **195–196**, 667–684.